Journal of Materials Chemistry C

New Ultrafast Scintillators with Core Valence Luminescence: Cs_2MgCl_4 and Cs_3MgCl_5

Journal:	*Journal of Materials Chemistry C*
Manuscript ID	TC-ART-03-2024-000877.R1
Article Type:	Paper
Date Submitted by the Author:	09-Apr-2024

Complete List of Authors:	Rutstrom, Daniel; University of Tennessee, Scintillation Materials Research Center; University of Tennessee, Materials Science and Engineering Stand, Luis; University of Tennessee, Scintillation Materials Research Center; University of Tennessee, Nuclear Engineering Windsor, Dylan; University of Tennessee, Materials Science and Engineering Xu, Haixuan; University of Tennessee, Materials Science and Engineering Kapusta, Maciej; Siemens Medical Solutions Melcher, Charles; University of Tennessee, Scintillation Materials Research Center; University of Tennessee, Nuclear Engineering Zhuravleva, Mariya; University of Tennessee, Scintillation Materials Research Center; University of Tennessee, Materials Science and Engineering

New Ultrafast Scintillators with Core Valence Luminescence: Cs_2MgCl_4 and Cs_3MgCl_5

Daniel Rutstrom,*[ab] Luis Stand,[ac] Dylan Windsor,[b] Haixuan Xu,[b] Maciej Kapusta,[d] Charles L. Melcher,[ac] Mariya Zhuravleva[ab]

Future experiments in high energy physics and medical imaging require radiation detectors having properties which are not presently available. The main limitations arise from lack of suitable scintillation crystals. This dilemma prompts the need for research leading to the discovery of new fast and bright scintillator materials that combine unique properties to fulfil modern experiment requirements without compromises. In this work, single crystals of Cs_2MgCl_4 and Cs_3MgCl_5 up to 12 mm in diameter are grown via the vertical Bridgman method. Scintillation properties are reported for the first time, and core valence luminescence is observed for both compounds. X-ray excited radioluminescence emission of Cs_2MgCl_4 is centered at 295 nm, with a scintillation decay time of 2.25 ± 0.05 ns and relatively high core-valence light yield of 2,200 ± 110 ph/MeV. Cs_3MgCl_5 has two main emission peaks centered at 242 nm and 302 nm, decay time of 1.46 ± 0.05 ns, and light yield of 1,340 ± 70 ph/MeV. The better coincidence time resolution (CTR) is obtained with Cs_2MgCl_4, which is measured to be 129 ± 4 ps FWHM. Density functional theory (DFT) calculations are also performed and provide supporting evidence that the observed scintillation originates from core valence luminescence. The combination of speed and brightness of these new scintillators could be useful for fast timing applications in which moderately dense materials are required.

1. Introduction

Inorganic scintillators are an important class of material for detecting ionizing radiation, converting X-rays or gamma rays, for example, into bursts of light that can be processed and analyzed to identify or localize the source of radiation. They are currently employed across a wide range of applications, each having a different set of performance criteria. These applications include nuclear security, high energy physics (HEP) experiments, medical imaging, space exploration, and oil well-logging. There is unfortunately no single scintillator that satisfies the requirements of all applications. Likewise, there are almost always tradeoffs when selecting from "off-the-shelf" scintillators, whether it be sacrificing performance or cost. Therefore, the search for new scintillators with potential to overcome limitations of existing materials is necessary to the development of next generation detection systems.

Fast scintillators (i.e. having short decay time) are desired in many detection applications, especially where excellent timing resolution is a key requirement (time-of-flight positron emission tomography (TOF-PET),[1-3] for example) or in high count rate environments where pulse pileup becomes an issue.[4-6] These applications also tend to require dense, high Z_{eff}, and radiation-hard materials, placing emphasis on inorganic over plastic scintillators despite the often favorable timing properties of the latter. So-called "fast" decay time (~20-40 ns) is commonly achieved by rare-earth ion doping in halides and oxides, usually with the Ce^{3+} activator ion. On the other hand, "ultrafast" decay time (~1 ns or less) in inorganic crystals is less frequently observed. Several ultrafast emission processes – Cherenkov emission,[7-10] hot intra-band luminescence,[11-13] and core valence luminescence [14-19] – are currently being explored as ways to improve the performance of detector systems used in fast timing applications, in particular by lowering the coincidence time resolution (CTR). Since the CTR is limited by the photon time density of the scintillation pulse, it follows that a combination of high light yield and short decay time are necessary for obtaining the best CTR. More specifically, $CTR \propto \sqrt{\tau_r \tau_d / N_{phe}}$, where τ_r and τ_d are the rise and decay times, respectively, and N_{phe} is the number of detected photoelectrons.

Compared to other ultrafast processes, core valence luminescence (CVL) is advantageous for use in a wider range of applications in that it produces significantly higher light yield (1,000-2,000 ph/MeV vs 10-40 ph/MeV).[2, 11, 20] A schematic illustration of the CVL mechanism is shown in Fig. 1. CVL can be observed in wide bandgap halide crystals if the condition $E_{vc} < E_g$ is satisfied, where E_{vc} is the energy difference between the top of the valence band and top of the outmost core level and E_g is the bandgap energy.[20] This condition is met in many fluorides and chlorides containing K^+, Cs^+, Rb^+, and/or Ba^{2+}, with the most notable example being BaF_2 – one of the few commercially available inorganic scintillators with a sub-nanosecond decay time. Despite its ultrafast timing capabilities, there is interest in finding alternatives to BaF_2 due to the drawbacks of its dominant slow decay component (630 ns) and spectral mismatch with common photodetectors resulting from its vacuum ultraviolet (VUV) emission.

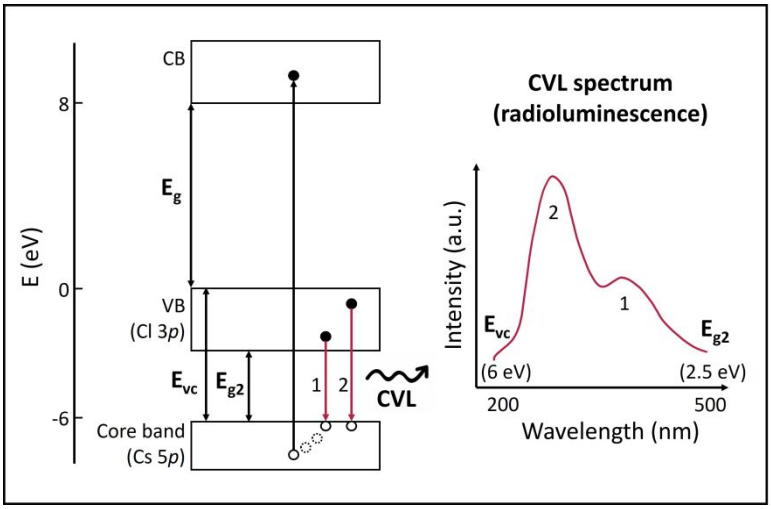

Fig. 1 Schematic illustration of the core valence luminescence mechanism for hypothetical CsCl-containing crystals. When X-rays or gamma rays interacting with a CVL crystal are of sufficient energy, an outermost core electron will be ejected to the conduction band leaving behind a core hole. The hole then relaxes to the top of the core level (mainly composed of the Cs 5*p* orbital in this case) where it can recombine with an electron from the valence band (mainly composed of the Cl 3*p* orbital in this case). The result is emission of photons with energies corresponding to transitions (1)-(2), which typically lie in the VUV to UV range of wavelengths.

We recently reported improvements to the scintillation properties of Cs_2ZnCl_4,[21] a CVL crystal with a relatively high light yield of ~2,000 ph/MeV and single-component decay time of 1.7 ns that shows potential as an alternative to BaF_2. Cs_3ZnCl_5 has also shown promise having a sub-nanosecond decay time of 0.8-0.9 ns.[21] The favorable properties of these materials have prompted us to search for new scintillators with similar structure and chemistry in an effort to (1) discover materials with superior light yield or decay time and (2) add to the list of known CVL materials so that relationships between composition, electronic structure, and scintillation properties can be better understood, possibly allowing higher-performance scintillators to be designed and developed more efficiently in the future.

So far, reports of core valence luminescence in compounds of the types Cs_2MCl_4 and Cs_3MCl_5 (M = alkaline earth metal or transition metal ion) are limited to Cs_2ZnCl_4,[21-26] Cs_2BaCl_4,[14, 27] and Cs_3ZnCl_5.[21, 24] Although structural and physical properties have been the topic of several studies,[28-30] there are no reports of scintillation properties for Cs_2MgCl_4 and Cs_3MgCl_5. Due to the presence of CsCl and compositional similarities to scintillators such as Cs_2ZnCl_4, Cs_3ZnCl_5, and $CsMgCl_3$,[14, 31, 32] we expect these compounds will also scintillate and show ultrafast core valence luminescence.

In this work, single crystals of Cs_2MgCl_4 and Cs_3MgCl_5 are grown by the vertical Bridgman technique and evaluated for use as gamma-ray or X-ray detectors. Phase analysis of the grown crystals is carried out using X-ray diffraction (XRD) to ensure the intended compounds are formed and that crystals are phase pure. Scintillation properties (radioluminescence, decay time, light yield) are characterized to determine if Cs_2MgCl_4 and Cs_3MgCl_5 crystals scintillate, assess how their performance compares to existing materials, and to confirm whether CVL is the mechanism responsible for scintillation. Due to the relevance to fast timing applications, coincidence time resolution (CTR) is also investigated. Finally, density functional theory (DFT) is used to calculate electronic band structures to determine if the energy condition ($E_{vc} < E_g$) required for CVL is satisfied for Cs_2MgCl_4 and Cs_3MgCl_5.

2. Experimental

2.1 Crystal Growth

Raw materials were purchased in the form of anhydrous beads of the binary halide salts CsCl (99.99%) and $MgCl_2$ (99.99%). Inside a nitrogen-filled glovebox, quartz ampoules were loaded with stoichiometric amounts of the constituent compounds – a 2:1 molar ratio of CsCl:$MgCl_2$ to form Cs_2MgCl_4 and a 3:1 molar ratio to form Cs_3MgCl_5. The loaded ampoules were then transferred to a vacuum drying system to ensure any residual moisture was driven off prior

[a] *Scintillation Materials Research Center, University of Tennessee, Knoxville, TN 37996, USA.*
[b] *Department of Materials Science and Engineering, University of Tennessee Knoxville, Knoxville, Tennessee, USA.*
[c] *Department of Nuclear Engineering, University of Tennessee Knoxville, Knoxville, Tennessee, USA.*
[d] *Siemens Medical Solutions, Rockford, Tennessee, USA*
† Footnotes relating to the title and/or authors should appear here.
Electronic Supplementary Information (ESI) available: [details of any supplementary information available should be included here]. See DOI: 10.1039/x0xx00000x

to synthesis. The raw materials were dried under dynamic vacuum at 100 °C for 12 hours, cooled to room temperature over a 1-hour period, and then sealed while still under vacuum using an oxy-hydrogen torch. Polycrystalline charges of Cs_2MgCl_4 and Cs_3MgCl_5 were then produced by heating above the melting points of CsCl (645 °C) and $MgCl_2$ (714 °C) for 12 hours followed by cooling to room temperature over several hours. This step was repeated 2-3 times to allow for complete mixing of the melt, inverting the ampoule between heating cycles. The same ampoule was used for both synthesis and crystal growth.

Single crystals 7 mm or 12 mm in diameter were grown in 2-zone or 3-zone furnaces using the vertical Bridgman method. The purpose of the larger diameter crystals was mainly to assess scalability of growth. A donut-shaped alumina baffle was positioned between the hot and cold zones of the furnaces to enhance the thermal gradients. The temperatures of the hot and cold zones were 595 °C and 345 °C, respectively, for Cs_2MgCl_4 (T_m = 545 °C) and were 630 °C and 380 °C, respectively, for Cs_3MgCl_5 (T_m = 527 °C). The ampoules were lowered through the furnace at a rate of 0.7-0.8 mm/hr for Ø7 mm crystals and 0.5 mm/hr for Ø12 mm crystals. The grown crystals were then cooled to room temperature at a rate of 5-7 °C/hr.

2.2 X-ray diffraction (XRD)

Phase analysis of the grown crystals was carried out with powder X-ray diffraction measured at room temperature. Data was collected from 15° to 70° 2-theta with a step size of 0.0066° 2-theta using a PANalytical Empyrean diffractometer with the Bragg-Brentano geometry and theta-theta goniometer. It was equipped with a Cu Kα X-ray source (1.5406 Å wavelength) operated at 45 kV and 40 mA. Powdered samples were loaded onto zero-background silicon holders while inside a glovebox and encapsulated with a Kapton film to prevent exposure to air during the measurements.

2.3 Differential scanning calorimetry (DSC)

Thermal analysis was performed to confirm congruent melting of the compounds. DSC was measured with a Setaram Labsys Evo using a heating and cooling rate of 5 K/min. Measurements were carried out with the samples (40 to 50 mg in mass) inside quartz crucibles that were sealed under vacuum to prevent volatilization and loss of stoichiometry.

2.4 Dynamic vapor sorption (DVS)

Hygroscopicity of the grown crystals was evaluated using a Surface Measurement Systems Intrinsic Plus DVS instrument. Samples were obtained in the form of single crystal chunks approximately 40 mg in mass. The crystals were placed into a sample chamber that was maintained at 40% relative humidity and room temperature, and the change in mass was recorded over a 5-hour period.

2.5 Scintillation properties

Characterization of scintillation properties (radioluminescence, decay time, light yield) was performed using small-sized pieces, typically Ø7 mm × 3 mm thick, that were cleaved from the grown crystals and polished with silicon carbide pads and mineral oil. Measurements were performed in air, and samples were repolished between measurements due to slight surface degradation from oxygen and moisture.

Radioluminescence was measured in a reflection geometry under excitation by an X-ray tube operated at 35 kV and 0.1 mA. The emission spectra were collected from 200 nm to 600 nm with a 150 mm focal length Acton SpectraPro 2150i monochromator and Hamamatsu R955 photomultiplier tube (PMT). A longpass optical filter was employed to allow measurements above 400 nm without interference from second order peaks. The emission spectra were not corrected for instrumental distortions, such as the monochromator throughput or detector sensitivity; however, the spectral response is relatively uniform across the measured wavelengths and is not expected to significantly affect any major features of the emission spectra of these samples. Scintillation decay time was measured under excitation by a 662 keV ^{137}Cs source using the time-correlated single photon counting technique described by Bollinger and Thomas using two Photonis XP2020Q PMTs.[33-35] A BaF_2 crystal (4 × 4 × 20 mm^3) was obtained from United Crystals and used as a standard reference for decay time measurements. Light yield was measured with the crystals covered or wrapped in sheets of reflective Teflon and coupled directly to a Hamamatsu R2059 PMT with a thin layer of mineral oil. Absolute light yield was determined using the method of Bertolaccini.[36] Additional experimental details for each setup can be found in [21].

2.6 Coincidence time resolution (CTR)

Coincidence time resolution (CTR) was measured with 3 × 3 × 5 mm^3 crystals (referred to hereon as "test" crystals) that were wrapped in Teflon and coupled to a Broadcom AFBR-S4N44C014M silicon photomultiplier (SiPM) with Viscasil optical grease. The SiPM bias voltage was set to 44.5 V. All test crystals were measured against a reference detector consisting of a 6 × 6 × 6 mm^3 LSO:Ce crystal and Hamamatsu H6610 PMT assembly, and the reference detector timing contribution of 135 ps FWHM was deconvolved from the measured results to obtain the CTR of the samples. During the measurements, a ^{68}Ge source placed between the test crystal and reference detector emits two 511 keV gamma rays in opposite directions that are detected in coincidence. Timing and energy signals from each detector were readout separately, and only events corresponding to the 511 keV photopeak in both the test crystal and reference detector were considered in the analysis. The experimental setup was similar to "Timing Setup A" described in [21], but with the SiPM replacing the "test detector" PMT. A simplified schematic is shown in Fig. 2.

In addition to Cs_2MgCl_4 and Cs_3MgCl_5, Cs_2ZnCl_4 and LSO:Ce,Ca test crystals (also 3 × 3 × 5 mm^3) were measured for comparison. Timing pickoff was performed using a custom-built leading edge (LE) discriminator with an externally electronically controlled threshold, and the samples were measured as the LE threshold was varied from 3 mV to 57 mV in increments of 6 mV. This increment was based on the value for a single photoelectron that was determined to be 8 mV prior to performing the measurements. For a more detailed description of the setup, the reader is referred to [21].

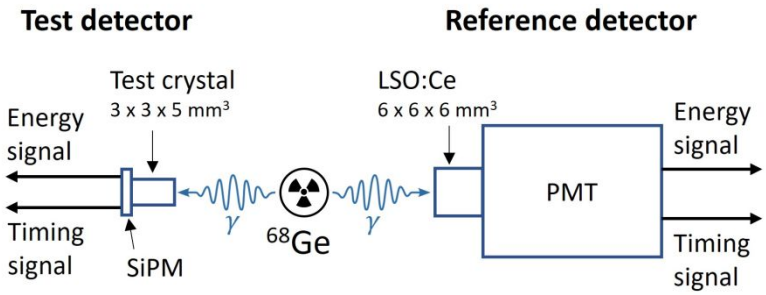

Fig. 2 Simple schematic of the setup used to measure CTR.

2.7 Density of states (DOS) calculations

Density functional theory (DFT) simulations were performed within the Vienna *ab initio* simulations package (VASP) to relax the structure and calculate the density of states (DOS).[37, 38] The generalized gradient approximation (GGA) functional PBEsol was used for all relaxations, while the DOS calculations were carried out using the Heyd-Scuseria-Ernzerhoff (HSE) screened hybrid functional with a Hartree – Fock range-separation parameter of 20% (HSE06).[39, 40] A single unit cell, containing 4 formula units, was used for both the Cs_2MgCl_4 and Cs_3MgCl_5 compounds with a Monhorst-Pack *k* point grid of 6 × 6 × 6 during relaxation and 4 × 4 × 4 during DOS calculations with hybrid functionals to reduce computational load while maintaining sufficient accuracy. The energy cutoff is 600 eV. Planar-augmented wave (PAW) basis [41] composed pseudopotentials are used for each species with the following valence electron configurations: Cs *3p3d4s* (9 e^-), Mg *2s* (10 e^-), and Cl *3s3p* (7 e^-). Each relaxation and self-consistent field calculation was converged to Hellmann-Feynman forces of <0.01 eV/Å and to a total energy difference of $<10^{-6}$ eV. The lattice constants found from published data in [28] and in [29] were used for the DOS calculations of Cs_2MgCl_4 and Cs_3MgCl_5. Comparatively, the lattice constants of each were calculated with DFT giving <2% error.

3. Results

3.1 Crystal growth, structural and physical properties

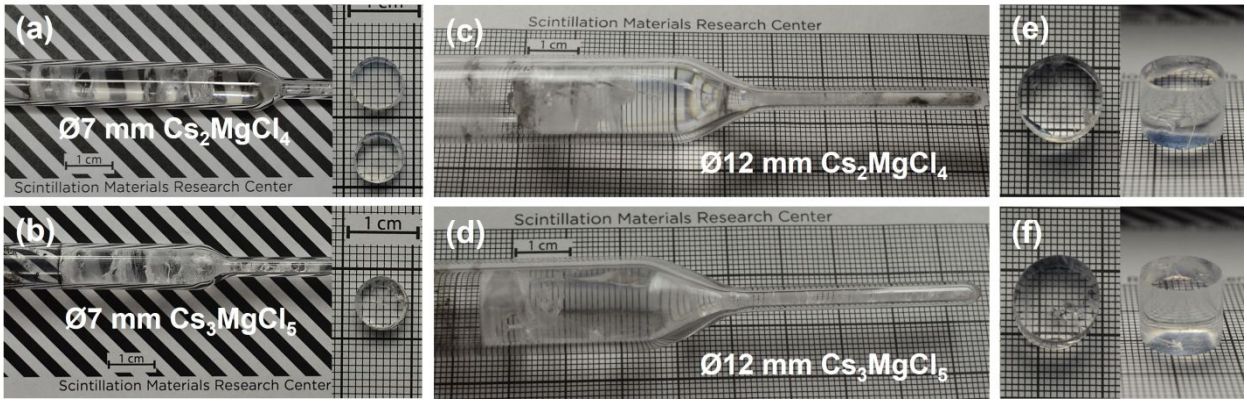

Fig. 3 Top row of photographs (a)(c)(e): Cs_2MgCl_4 crystals. Bottom row of photographs (b)(d)(f): Cs_3MgCl_5 crystals. (a)(b) as-grown (left) Ø7 mm crystals and ~4 mm thick slabs (right) that were cleaved from the boules and polished. (c)(d) as-grown Ø12 mm crystals. (e)(f) ~10 mm tall cylinders cut from the Ø12 mm boules and polished.

Fig. 3 shows photographs of the grown Cs_2MgCl_4 and Cs_3MgCl_5 crystals. The crystals are colorless and transparent with some minor cracking mostly near the surface. Cracking appears to be worse in the A_3MX_5-type crystal, which is also what we observed previously for the Zn-containing analogues.[21] Based on these observations, Cs_2MgCl_4 may be the more promising crystal for scale up purposes. Optimization of growth parameters for both crystals would likely yield better results (i.e. less cracking), but this was outside the scope of the present work.

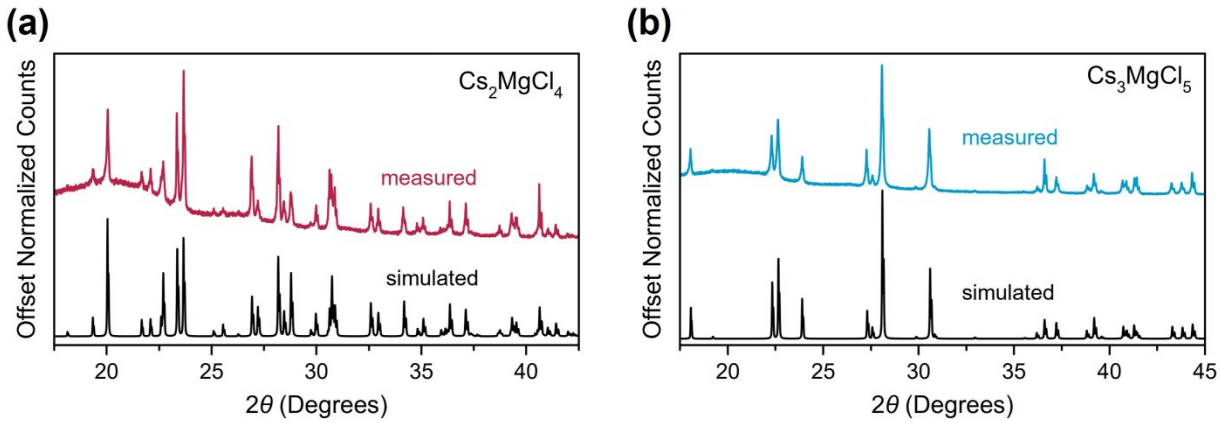

Fig. 4 (a) Measured powder XRD pattern of Cs_2MgCl_4 compared to the simulated pattern generated using the Vesta software package. (b) Measured powder XRD pattern of Cs_3MgCl_5 compared to the simulated pattern generated using the Vesta software package.[42] The broad amorphous peak around 20° originates from the protective Kapton film.

XRD measurements confirmed the phase purity of the grown crystals. The orthorhombic crystal structure (space group *Pnma*) was obtained for Cs_2MgCl_4, which is apparent from matching measured and simulated patterns in Fig. 4a. The reported lattice parameters of Cs_2MgCl_4 are a = 9.777(4) Å, b = 13.234(6) Å, and c = 7.514(3) Å (V = 972.23 Å^3) and the calculated density is 2.95 g/cm^3.[28] The structure consists of isolated $[ZnCl_4]^{2-}$ tetrahedra and two separate Cs sites with coordination numbers (CN) of CN = 8 and CN = 9 for the Cs1 and Cs2 sites, respectively. The structure and space group are the same as those of the CVL scintillator Cs_2ZnCl_4, which has a slightly smaller unit cell with lattice parameters a = 9.7577(15) Å, b = 12.9704(16) Å, and c = 7.4004(10) Å (V = 936.6 Å^3) despite the larger ionic radius of Zn^{2+} (0.6 Å for CN = 4) compared to Mg^{2+} (0.57 Å for CN = 4).[43, 44]

The measured XRD pattern for the Cs_3MgCl_5 crystal also matches closely with the simulated pattern, as can be seen in Fig. 4b. Cs_3MgCl_5 is isostructural with the CVL scintillator Cs_3ZnCl_5, both adopting the tetragonal structure (space group I_4/mcm). This structure also consists of isolated $[ZnCl_4]^{2-}$ tetrahedra and two separate Cs sites, but in this case with CN = 8 and CN = 10 for the Cs1 and Cs2 sites, respectively. The reported lattice parameters of Cs_3MgCl_5 are $a = b =$ 9.23 Å and c = 14.88 Å (V = 1267.67 Å^3) and its calculated density is 3.14 g/cm^3.[29] Similar to the A_2MX_4 compounds, the unit cell volume for the Zn-containing compound is smaller than that of the Mg-containing despite the larger ionic radius of Zn^{2+}. Lattice parameters for the isostructural Cs_3ZnCl_5 are $a = b$ = 9.2421(18) Å and c = 14.4928(15) Å (V = 1237.92 Å^3).[45] This data is summarized in Table 1.

Table 1. Crystal structures and reported lattice parameters of Cs_2MgCl_4 and Cs_3MgCl_5 compared to those of CVL scintillators Cs_2ZnCl_4 and CS_3ZnCl_5.

Composition	Crystal structure	Lat. Param., *a* (Å)	Lat. Param., *b* (Å)	Lat. Param., *c* (Å)	Ref.
Cs_2ZnCl_4	orthorhombic	9.7577(15)	12.9704(16)	7.4004(10)	43
Cs_2MgCl_4	orthorhombic	9.777(4)	13.234(6)	7.514(3)	28
Cs_3ZnCl_5	tetragonal	9.2421(18)	9.2421(18)	14.4928(15)	45
Cs_3MgCl_5	tetragonal	9.23	9.23	14.88	29

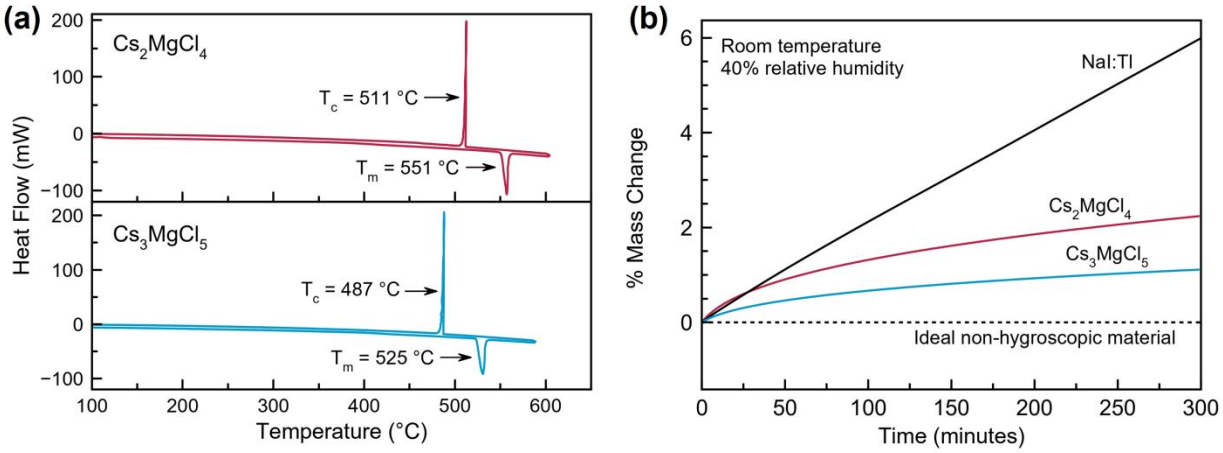

Fig. 5 (a) DSC curves showing the melting and solidification behavior of Cs_2MgCl_4 and Cs_3MgCl_5. The endothermic direction is down. (b) DVS water sorption curves of Cs_2MgCl_4 and Cs_3MgCl_5 at 40% relative humidity compared with NaI:Tl.

DSC of Cs_2MgCl_4 and Cs_3MgCl_5 was measured to confirm the reported congruent melting of these compounds, [46-49] which is favorable for melt growth techniques such as the Bridgman method. A single endothermic and single exothermic peak are observed in the DSC curves of each (Fig. 5a) indicating congruent melting (a eutectic reaction can be ruled out per results of XRD). Also evident from DSC is the lack of any solid-solid structural phase transitions, which can negatively impact optical transparency or cause stress-induced cracking during post-growth cooling of the crystal. Melting points were also determined from DSC and are consistent with reported values. The onset of melting measured for Cs_2MgCl_4 was 551 °C (lit.,[46] T_m = 545 °C) and for Cs_3MgCl_5 was 525 °C (lit.,[46] T_m = 527 °C).

DVS measurements reveal that Cs_2MgCl_4 and Cs_3MgCl_5 are slightly hygroscopic. This is apparent from Fig. 5b, which shows a ~2.4% mass gain for Cs_2MgCl_4 and ~1.1% mass gain for Cs_3MgCl_5 after 5 hours at 40% relative humidity at room temperature. Compared to many other common halide scintillators (NaI:Tl, for example), this is still a relatively low degree of hygroscopicity. While performing measurements of scintillation properties with samples exposed to air for ~30 minutes at a time, the only noticeable effect was the formation of a thin white film on the surface that made the crystals appear more translucent. However, this film was easily polished away. To verify that the hydrated layer had no effect on the measured scintillation properties, a light yield measurement was performed in air over an 18-hour period with no change in photopeak shape or position observed (Figure S1). Additionally, during overnight CTR measurements, the first few data points (i.e. first few LE values) were repeated after completing the initial series to verify the performance had not changed due to long term air exposure. In the case of overnight measurements, the optical coupling (mineral oil or Viscasil optical grease) preserved the transparency of the crystal face in contact with the

photosensor, allowing the emitted light to escape despite the sides and top of the crystal turning opaque. Given that Cs_2MgCl_4 and Cs_3MgCl_5 are considerably less hygroscopic than the widely employed NaI:Tl, simple hermetic packaging methods would allow their use in real detector systems without major concerns of instability.

3.2 Scintillation properties

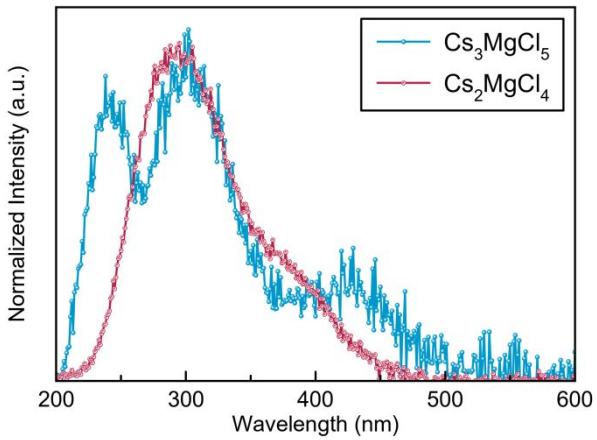

Fig. 6 Radioluminescence emission spectra of Cs_2MgCl_4 and Cs_3MgCl_5 crystals at room temperature.

Fig. 6 shows the X-ray excited emission spectra (radioluminescence) of Cs_2MgCl_4 and Cs_3MgCl_5. To our knowledge, this is the first instance of scintillation reported for either compound. The emission being primarily positioned in the UV region is consistent with CVL observed in other CsCl-based crystals.[14, 31, 50, 51] Likewise, the longer wavelength emission of Cs_2MgCl_4 and Cs_3MgCl_5 compared to fluoride materials (such as BaF_2) is beneficial when considering compatibility with commonly used SiPMs and PMTs that have poor spectral sensitivity in the VUV region where many fluorides emit.

The dominant emission band for Cs_2MgCl_4 is centered near 295 nm, with a lower intensity shoulder around 360 nm (Fig. 6). Besides having slightly broader less resolved peaks and being redshifted by several nm, the position and structure closely resemble the emission spectrum of the CVL scintillator Cs_2ZnCl_4.[21] The emission spectrum of Cs_3MgCl_5 on the other hand consists of two main bands with maxima at 242 nm and 302 nm, with a third band near 425 nm. Similarly, three emission bands with nearly identical position and structure are observed with the Zn-containing analogue, Cs_3ZnCl_5.[21]

It has been established that the number of peaks in the CVL emission spectrum depends on the CN of the CVL-active cation, with the spectra becoming more complicated as CN increases from CN = 6 (1 band) to CN = 8 (2 bands) to CN = 12 (complex structure).[20, 52] This could explain why the number of emission bands differs between the A_2MX_4-type crystals (2 bands) and A_3MX_5-type crystals (3 bands). As discussed in Section 3.1, both structures contain two separate Cs sites, however, the CN for the Cs2 site is larger in the A_3MX_5-type structure (CN = 10) than in the A_2MX_4-type structure (CN = 9). Additionally, given that CVL spectra are known to reflect the valence band density of states,[20] these results might indicate similar electronic band structures for the analogous Mg- and Zn-containing crystals if in fact the scintillation in Cs_2MgCl_4 and Cs_3MgCl_5 also originates from CVL.

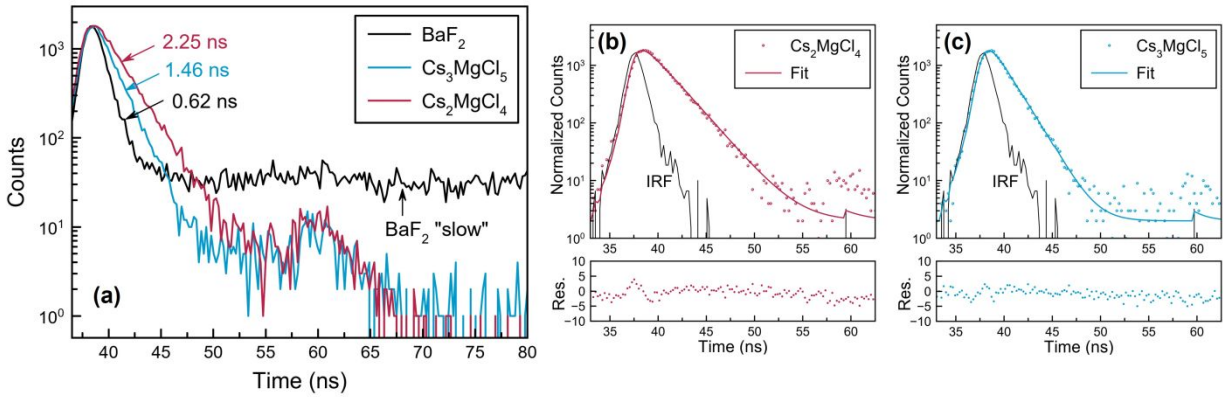

Fig. 7 (a) Scintillation decay profile of Cs_2MgCl_4 and Cs_3MgCl_5 compared with a reference BaF_2 crystal. The feature between 55 ns to 65 ns for Cs_2MgCl_4 and Cs_3MgCl_5 is an instrumental artifact. (b) and (c) show the fitted decay profiles, where the fits represent the convolution of the instrument response (IRF) with a single-exponential function.

The measured scintillation decay time profiles of Cs_2MgCl_4 and Cs_3MgCl_5 are shown in Fig. 7a, along with a BaF_2 reference (United Crystals), with both crystals exhibiting ultrafast timing characteristics typical of CVL. The decay constants of Cs_2MgCl_4 and Cs_3MgCl_5 were determined to be 2.25 ± 0.05 ns and 1.46 ± 0.05 ns, respectively. The decay constant for the fast component of BaF_2 was determined to be 0.62 ± 0.05 ns and agrees closely with the established range between 0.6 ns and 0.8 ns reported in literature. The time constants were obtained by fitting a convolution of the instrumental response with a single-exponential function for Cs_2MgCl_4 and Cs_3MgCl_5 (Fig. 7b and Fig. 7c) and double-exponential function for BaF_2. No long components were visible in the decay profiles of Cs_2MgCl_4 and Cs_3MgCl_5 when measured over longer time windows, an example of which can be seen in Figure S2. The absence of any slow components for Cs_2MgCl_4 and Cs_3MgCl_5 is advantageous for high count rate environments in which pulse pile up must be avoided and where the slow component of BaF_2 (630 ns) is problematic.

The decay times of Cs_2MgCl_4 and Cs_3MgCl_5 are comparable to other ternary CsCl-based CVL crystals, providing further evidence that the emission can be attributed to core valence luminescence. Examples include $CsCaCl_3$ (2.47 ns),[14] $CsMgCl_3$ (2.36 ns),[14] Cs_2BaCl_4 (1.68 ns),[14] Cs_2ZnCl_4 (1.66 ns),[21] and Cs_3ZnCl_5 (0.82 ns).[21] Similar to the Zn-containing analogues, faster decay time is observed with Cs_3MgCl_5 than with Cs_2MgCl_4, hinting that the A_3MX_5-type family of compounds could be the key to discovering additional inorganic scintillators with sub-ns decay time, for which few are currently known to exist.

Table 2. Average Cs–Cl bond lengths and decay constants for CsCl, $CsMgCl_3$, and other known CVL scintillators of the types A_3MX_5 (space group *I*4/*mcm*) and A_2MX_4 (space group *Pnma*). The compound Cs_2BaCl_4 is excluded from the list due to its dissimilar crystal structure (cubic, space group *I*-43*d*), in which Cs^+ and Ba^{2+} (both CVL-active ions) occupy the same crystallographic site, that may additionally influence the CVL properties.[53] Average bond lengths were determined using the Vesta software package and published structural data.[42] For structures with two Cs sites, the total average is weighted based on CN.

Composition	Decay Constant (ns)	Ref.	Cs1 Average Cs–Cl bond length (Å)	Cs2 Average Cs–Cl bond length (Å)	Average Cs–Cl bond length (Å)	Ref.
CsCl	0.88	[54]	-	-	3.564	[55]
Cs_3ZnCl_5	0.82 – 1.1	[21, 24]	3.536	3.778	3.670	[45]
Cs_3MgCl_5	1.46	this work	3.563	3.804	3.697	[29]
Cs_2ZnCl_4	1.6 – 1.7	[21, 22, 24]	3.7518	3.518	3.663	[43]
Cs_2MgCl_4	2.25	this work	3.767	3.608	3.683	[28]
$CsMgCl_3$	2.1 – 2.36	[14, 31]	-	-	3.728	[56]

From these results, it is apparent that for both the A_2MX_4 and A_3MX_5 structure types, full replacement of Zn^{2+} with Mg^{2+} leads to lengthening of the decay time. According to Rodnyi, as the A–X distance increases when changing from an AX to AMX_3 CVL crystal (ex. – Cs to Cl distance from CsCl to $CsMgCl_3$), decay time and light yield will increase due to a smaller overlap of the wave functions of A^+ and X^- ions and therefore a lower probability of radiative CVL transitions.[57] This relationship has been discussed in other works as well, including [31, 58, 59]. To determine whether the trend holds for

the A_3MX_5-type (space group I_4/mcm) and A_2MX_4-type (space group *Pnma*) compounds, decay constants and average Cs–Cl bond lengths were compiled and are listed in Table 2 along with those of CsCl and $CsMgCl_3$. It should be noted that the AX and AMX_3-type compounds are a simpler case given that only one crystallographic site exists for Cs ions whereas two sites exist in the A_2MX_4-type and A_3MX_5-type compounds (as discussed in Section 3.1).

When looking solely at the Cs1 site, the trend with decay time appears to be consistent across Cs_3ZnCl_5, Cs_3MgCl_5, Cs_2ZnCl_4, and Cs_2MgCl_4, which show lengthening decay times with increasing bond length. Likewise, the same is true when replacing Zn^{2+} with Mg^{2+} in a given structure type regardless of which site is considered. However, a clear trend is not observed across all compositions for the Cs2 site or the total average bond length. We speculate one possibility for this result could be that the Cs1 site somehow plays a more prominent role in the CVL process than the Cs2 site in these compounds, however, this has not been verified. Most likely there are more complex factors contributing to the scintillation kinetics in the materials studied in the present work, and further investigation is necessary to draw definitive conclusions about the differences in decay times and how they relate to the Cs–Cl distances. In an investigation of impurity-induced CVL in CaF_2:Ba and SrF_2:Ba, Terekhin et al. also did not observe the expected acceleration of decay time despite the smaller Ba–F distances in the doped compounds compared to BaF_2 and point out that the probability of optical transitions is not only determined by the CVL-active cation to halogen anion distance, but also by the shape of the respective wave functions.[59]

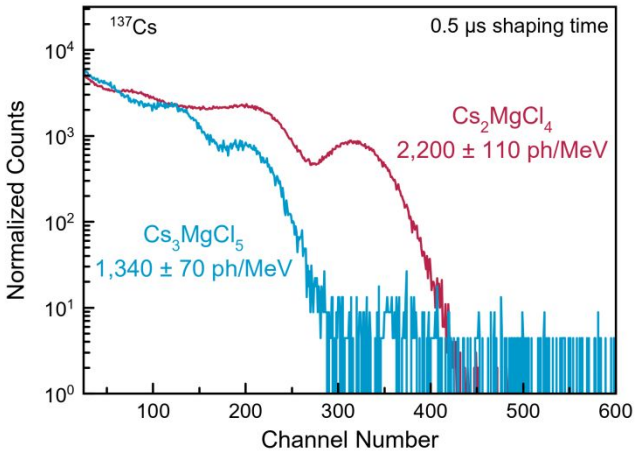

Fig. 8 Pulse height spectra of Ø7 mm × 3 mm Cs_2MgCl_4 and Cs_3MgCl_5 crystals measured with a 662 keV ^{137}Cs source.

Pulse height spectra for small-sized crystals of Cs_2MgCl_4 and Cs_3MgCl_5 are shown in Fig. 8. The full-energy (662 keV) deposition photopeaks can be resolved for both. Measurements were performed at various shaping times to verify the absence of long decay components (on the order of a few hundred nanoseconds or greater) that were not visible in the scintillation decay profiles. No significant change in photopeak position was observed when collecting spectra with shaping time ranging from 0.5 to 10 µs, which provides further evidence that there is no significant contribution from long components in the time profiles of these crystals. Light yield was measured to be 2,200 ± 110 ph/MeV for Cs_2MgCl_4 and 1,340 ± 70 ph/MeV for Cs_3MgCl_5. These values are similar to those of the Zn-containing analogues (1,980 ± 100 ph/MeV for Cs_2ZnCl_4 and 1,460 ± 70 ph/MeV for Cs_3ZnCl_5), in which the A_2BX_4-type crystal was also the brighter of the two, indicating another possible connection between crystal structure and CVL properties. Cs_2MgCl_4 has a relatively high light yield compared to many other CVL materials, which are mostly below 1,500 ph/MeV.[14, 15, 20, 51] This higher light yield, or brightness, becomes especially important in applications requiring good timing resolution given that the coincidence time resolution (CTR) is inversely proportional to the square root of the number of detected photons, as discussed in the introduction.

3.3 Coincidence time resolution (CTR)

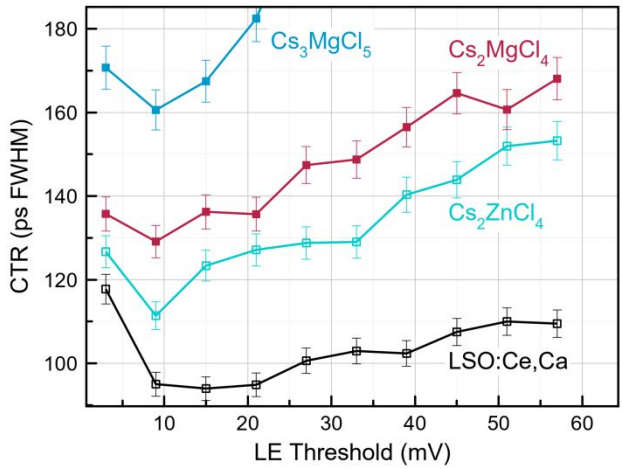

Fig. 9 CTR measurements of Cs_2MgCl_4 and Cs_3MgCl_5 compared to reference samples of Cs_2ZnCl_4 and LSO:Ce,Ca. All crystals were approximately 3 × 3 × 5 mm³.

The CTR for 3 × 3 × 5 mm³ samples measured as a function of leading edge (LE) threshold is shown in Fig. 9. LSO:Ce,Ca and Cs_2ZnCl_4 are included for comparison, with LSO:Ce,Ca considered as the state-of-the-art and Cs_2ZnCl_4 being a known CVL material. The same Cs_2ZnCl_4 crystal from [21] that we reported to have a CTR of 148 ± 1 ps FWHM was again measured, however, a better CTR of 111 ± 3 ps FWHM was achieved in the present work and is attributed to replacement of the test detector PMT with the SiPM (as described in Section 2.6). The LSO:Ce,Ca crystal had a CTR of 94 ± 3 ps FWHM. Based on the ratios of decay time to light yield, it is expected that Cs_2MgCl_4 and Cs_3MgCl_5 should have CTR values slightly larger than Cs_2ZnCl_4 by approximately 10% and 14%, respectively (see Table 3). The measured CTR for Cs_2MgCl_4 was 129 ± 4 ps FWHM, or about 16% larger than that of Cs_2ZnCl_4. This result agrees well with the expected 10% and demonstrates the excellent timing capabilities of Cs_2MgCl_4. On the other hand, Cs_3MgCl_5 did not perform as well as expected. The measured CTR was 161 ± 5 ps FWHM, or about 45% larger than that of Cs_2ZnCl_4. A possible explanation is that this difference arises due to the different emission spectra of Cs_2MgCl_4 and Cs_3MgCl_5. More specifically, a larger fraction of the light is emitted below 275 nm for Cs_3MgCl_5 (Fig. 6), and the photon detection efficiency (PDE) of the SiPM dips below 10% near 275 nm compared to ~35% near 300 nm. Likewise, the significantly better CTR achieved with LSO:Ce,Ca likely results from a combination of its higher photon time density (Table 3) and the higher PDE of the SiPM (>60% at 420 nm) in the spectral region where LSO:Ce,Ca emits. Future experiments making use of novel VUV-sensitive SiPMs could potentially lead to further improvements to the CTR of these CVL materials.

Table 3. Relevant properties of Cs_2MgCl_4 and Cs_3MgCl_5 and comparison of CTR with Cs_2ZnCl_4. CTR values are for the optimal LE threshold, which was at 9 mV for each.

Composition	τ (ns)	LY at 662 keV (ph/MeV)	LY/τ (ph/meV/ns)	$\frac{\sqrt{\tau/LY}}{(\sqrt{\tau/LY})_{Cs2ZnCl4}}$	measured CTR (ps FWHM)	expected CTR (ps FWHM)
Cs_2ZnCl_4	1.66 [21]	1,980 [21]	1,193	1	111 ± 3	-
Cs_2MgCl_4	2.25 ± 0.05	2,200 ± 110	978	1.10	129 ± 4	123
Cs_3MgCl_5	1.46 ± 0.05	1,340 ± 70	918	1.14	161 ± 5	127
LSO:Ce,Ca	31.5 ± 0.5	39,800 ± 2,000	1,263	0.97	94 ± 3	108

3.4 Density of states (DOS) calculations

Density functional theory (DFT) calculations were performed for Cs_2MgCl_4 and Cs_3MgCl_5 to establish the potential for core valence luminescence based on electronic band structures of these compounds. Similar methods have been used to investigate CVL in other materials, such as $CsMgCl_3$,[32] $CsCaCl_3$,[60] $KMgF_3$,[61] LaF_3,[62] and $KMgCl_3$.[63] In the present work, these calculations are useful for two primary reasons: (1) to determine if the criteria $E_{vc} < E_g$ is satisfied, indicating that core valence luminescence is energetically possible and (2) to compare some features of the calculated density of states (DOS) to measured emission spectra since the CVL spectrum (radioluminescence) should reflect the valence band DOS.[20, 64] This fact is apparent when considering that the emitted light must fall within the range of energies corresponding to transitions from the top and bottom of the valence band to the top of the outermost core band (Fig. 1). Put more simply, the low energetic edge of the CVL emission spectrum should correspond to the parameter E_{g2}. The high energetic edge of the CVL spectrum should correspond to the parameter E_{vc}.

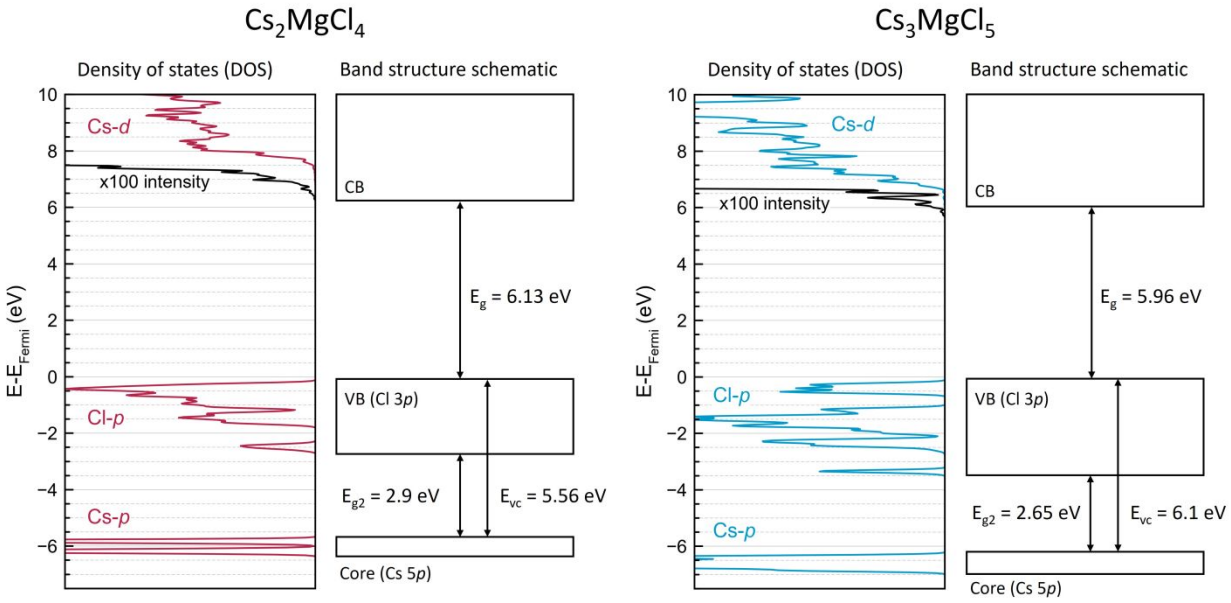

Fig. 10 Calculated partial density of states (DOS) and schematic band diagrams with relevant energies for CVL labeled.

Fig. 10 shows the calculated partial density of states (PDOS) for Cs_2MgCl_4 and Cs_3MgCl_5 along with schematic illustrations of the band structures. The valence band is primarily composed of Cl-*p* states for both compounds, while the outermost core level is composed mainly of Cs-*p* states. It is apparent that the necessary condition $E_{vc} < E_g$ is satisfied for Cs_2MgCl_4 (E_{vc} = 5.56 eV and E_g = 6.13 eV), further supporting the experimental results that suggest CVL as the scintillation mechanism. Based on the DOS, CVL is expected to occur through radiative transitions between Cs 5*p* holes and Cl 3*p* electrons, as is typical for CsCl-based CVL crystals.

Interpretation of the data in Fig. 10 is straightforward for Cs_2MgCl_4, as E_{vc} = 5.56 eV is clearly less than E_g = 6.13 eV. The story is less obvious with Cs_3MgCl_5, where the DOS shows a very close difference between E_{vc} and E_g; however, the values of these parameters overlap only for a small part of the Brillouin zone. In this system, the Cs-*p* states are ~6.1 eV below the valence band maximum (VBM), the Cl-*p* states are at the VBM, and the Cs-*d* states make up the conduction band minimum (CBM) at 5.96 eV. At a particular k-point within the Brillouin zone, each of these states has an energy window over which the Kohn-Sham states (the bands in DFT) vary, leading to a variation in the values of E_{vc} (between 5.99 eV and 6.13 eV) and E_g (between 5.96 eV and 7.29 eV). Calculating these two energy differences at every k-point has shown $E_{vc} < E_g$ for ~89% of the Brillouin zone and is at most 0.17 eV larger in the other 11%. Additionally, Yang *et. al.* [65] found that HSE underestimates large band gaps. These results suggest that CVL is possible for Cs_3MgCl_5 as well, as was inferred from the experimental data.

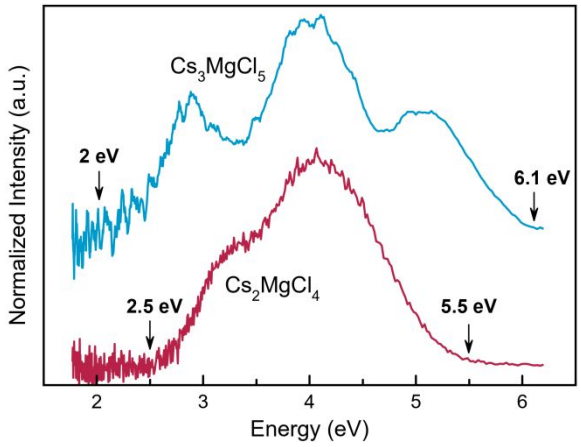

Fig. 11 Emission spectra converted to energy scale highlighting the low energetic and high energetic edges of CVL that correspond to the parameters E_{g2} and E_{vc}, respectively.

Radioluminescence spectra were converted from wavelength to energy (Fig. 11) to allow comparison with the energy parameters E_{g2} and E_{vc} obtained from the calculated DOS. The Jacobian transformation was applied during the conversion, which scales intensity values in order to correct for the uneven interval spacings between wavelength and energy scales.[66] The low energetic and high energetic edges of CVL in both cases were approximated as the peak onsets. The calculated parameters agree reasonably well with the measured CVL edges of 2.5 eV (E_{g2} = 2.9 eV) and 5.5 eV (E_{vc} = 5.56 eV) for Cs_2MgCl_4. There is also good agreement between calculated and measured values for Cs_3MgCl_5, for which the low and high energetic edges of CVL are 2 eV (E_{g2} = 2.65 eV) and 6 eV (E_{vc} = 6.1 eV). The small discrepancy between calculated and experimental values for E_{g2} may be a result of thermal broadening of the valence band. The larger VB width for Cs_3MgCl_5 compared to Cs_2MgCl_4 in the calculated DOS (Fig. 10) also agrees well with the experimental data in which Cs_3MgCl_5 has the broader emission spectrum, spanning a wider energy range.

4. Conclusions

Cs_2MgCl_4 and Cs_3MgCl_5 were explored as potential new scintillator materials. Single crystals of each were grown using the Bridgman method, and scintillation was observed for both compounds under X-ray and gamma ray excitation. The ultrafast scintillation decay times (2.25 ± 0.05 ns for Cs_2MgCl_4 and 1.46 ± 0.05 ns for Cs_3MgCl_5) and radioluminescence emission spectra that are consistent with other CVL materials suggest that scintillation in both crystals arises from core valence luminescence. DFT calculations provided further evidence of CVL, illustrating that the necessary energy condition is satisfied ($E_{vc} < E_g$) and that the low and high energetic edges of the measured emission spectra show good agreement with the calculated valence band DOS. Several parallels were observed between Cs_2MgCl_4 and Cs_3MgCl_5 and the previously studied compounds Cs_2ZnCl_4 and Cs_3ZnCl_5, revealing a possible connection between crystal structure and CVL properties in these two systems. Specifically, (1) the emission spectra are nearly identical for the compounds of the same structure type (2) the A_2MX_4-type compound is the brighter of the two in both cases and (3) the A_3MX_5-type compound is the faster of the two in both cases.

The relationship between structure, cation species, and the characteristics of core valence luminescence is still not well-established in ternary compounds besides those of the AMX_3 type. The results reported here could help provide a more complete picture of the possible structural and compositional dependencies of CVL for a wider range of materials. Like the Zn-containing analogues, Cs_2MgCl_4 and Cs_3MgCl_5 can also potentially offer advantages over the current state-of-the-art ultrafast scintillator BaF_2, including longer wavelength emission and absence of long decay components. Strategies for improving performance of these materials by means of compositional engineering will be the topic of future work.

Disclaimer

Author contributions

Daniel Rutstrom: conceptualization, methodology, data curation, validation, formal analysis, investigation, writing – original draft, writing – review & editing, visualization. **Luis Stand:** conceptualization, validation, supervision, writing – review & editing. **Dylan Windsor:** software, methodology, data curation, formal analysis, writing – review & editing. **Haixuan Xu:** software, funding acquisition, resources, writing – review & editing. **Maciej Kapusta:** methodology, data curation, validation, formal analysis, writing – review & editing. **Charles L. Melcher:** conceptualization, supervision, funding acquisition, resources, writing – review & editing. **Mariya Zhuravleva:** conceptualization, project administration, supervision, funding acquisition, resources, writing – review & editing.

Conflicts of Interest

There are no conflicts of interest to declare.

Acknowledgements

This material is based upon work supported by the Department of Energy National Nuclear Security Administration through the Nuclear Science and Security Consortium under Award Number DE-NA-0003996. XRD was performed at the Institute for Advanced Materials and Manufacturing (IAMM). D.W. and H.X. were supported by the National Science Foundation Materials Research Science and Engineering Center program through the UT Knoxville Center for Advanced Materials and Manufacturing (DMR-2309083).

References

1. L. M. Fraile, V. Sánchez-Tembleque, J. Benito, M. García-Díez, J. M. Udías and V. Vedia, *Nuclear Instruments and Methods in Physics Research Section B: Beam Interactions with Materials and Atoms*, 2020, **463**, 394-397.
2. S. Gundacker, R. Martinez Turtos, N. Kratochwil, R. H. Pots, M. Paganoni, P. Lecoq and E. Auffray, *Physics in Medicine & Biology*, 2020, **65**, 025001.
3. F. Pagano, N. Kratochwil, M. Salomoni, M. Pizzichemi, M. Paganoni and E. Auffray, *Physics in Medicine & Biology*, 2022, **67**, 135010.
4. C. Hu, L. Zhang, R.-Y. Zhu, A. Chen, Z. Wang, L. Ying and Z. Yu, *Nuclear Instruments and Methods in Physics Research Section A: Accelerators, Spectrometers, Detectors and Associated Equipment*, 2020, **950**, 162767.
5. C. Hu, L. Zhang, R.-Y. Zhu, M. Demarteau, R. Wagner, L. Xia, J. Xie, X. Li, Z. Wang, Y. Shih and T. Smith, *Nuclear Instruments and Methods in Physics Research Section A: Accelerators, Spectrometers, Detectors and Associated Equipment*, 2019, **940**, 223-229.
6. Z. Wang, E. Guardincerri, D. Rathman, M. Azzouz, C. Barnes, R. Berger, E. Bond, D. Craig, D. Holtkamp, J. Kapustinsky, A. Klimenko, K. Kwiatkowski, R. Merl, C. Morris, J. Perry, E. Ramberg, R. Reich, A. Ronzhin, K. Warner, R. Williams and R.-Y. Zhu, *Gigahertz (GHz) hard x-ray imaging using fast scintillators*, SPIE, 2013.
7. D. A. Finogeev, V. A. Grigoriev, V. A. Kaplin, O. V. Karavichev, T. L. Karavicheva, A. S. Konevskikh, A. B. Kurepin, A. N. Kurepin, V. A. Loginov, A. I. Mayevskaya, Y. A. Melikyan, I. V. Morozov, D. V. Serebryakov, A. I. Shabanov, M. Slupecki, A. A. Tikhonov and W. H. Trzaska, *Journal of Physics: Conference Series*, 2017, **798**, 012168.
8. R. Latella, A. J. Gonzalez, D. A. B. Bonifacio, M. Kovylina, A. Griol, J. M. Benlloch, P. Lecoq and G. Konstantinou, *IEEE Transactions on Radiation and Plasma Medical Sciences*, 2023, DOI: 10.1109/TRPMS.2023.3310581, 1-1.
9. M. Miyata, H. Tomita, K. Watanabe, J. Kawarabayashi and T. Iguchi, *Journal of Nuclear Science and Technology*, 2006, **43**, 339-343.
10. R. Ota, K. Nakajima, T. Hasegawa, I. Ogawa and Y. Tamagawa, *Nuclear Instruments and Methods in Physics Research Section A: Accelerators, Spectrometers, Detectors and Associated Equipment*, 2019, **923**, 1-4.
11. S. I. Omelkov, V. Nagirnyi, S. Gundacker, D. A. Spassky, E. Auffray, P. Lecoq and M. Kirm, *Journal of Luminescence*, 2018, **198**, 260-271.

12. S. I. Omelkov, V. Nagirnyi, A. N. Vasil'ev and M. Kirm, *Journal of Luminescence*, 2016, **176**, 309-317.
13. J. Saaring, A. Vanetsev, K. Chernenko, E. Feldbach, I. Kudryavtseva, H. Mändar, S. Pikker, R. Pärna, V. Nagirnyi, S. Omelkov, I. Romet, O. Rebane and M. Kirm, *Journal of Luminescence*, 2022, **244**, 118729.
14. V. Vaněček, J. Páterek, R. Král, R. Kučerková, V. Babin, J. Rohlíček, R. Cala', N. Kratochwil, E. Auffray and M. Nikl, *Optical Materials: X*, 2021, **12**, 100103.
15. V. Khanin, I. Venevtsev and P. Rodnyi, *Optical Materials*, 2023, **136**, 113399.
16. K. Takahashi, M. Koshimizu, Y. Fujimoto, T. Yanagida and K. Asai, *Nuclear Instruments and Methods in Physics Research Section A: Accelerators, Spectrometers, Detectors and Associated Equipment*, 2020, **954**, 161842.
17. R. H. Pots, E. Auffray and S. Gundacker, *Frontiers in Physics*, 2020, **8**.
18. K. Herweg, V. Nadig, V. Schulz and S. Gundacker, *IEEE Transactions on Radiation and Plasma Medical Sciences*, 2023, **7**, 241-252.
19. K. Yamanoi, R. Nishi, K. Takeda, Y. Shinzato, M. Tsuboi, M. V. Luong, T. Nakazato, T. Shimizu, N. Sarukura, M. Cadatal-Raduban, M. H. Pham, H. D. Nguyen, S. Kurosawa, Y. Yokota, A. Yoshikawa, T. Togashi, M. Nagasono and T. Ishikawa, *Optical Materials*, 2014, **36**, 769-772.
20. P. A. Rodnyi, *Radiat. Meas.*, 2004, **38**, 343-352.
21. D. Rutstrom, L. Stand, C. Delzer, M. Kapusta, J. Glodo, E. van Loef, K. Shah, M. Koschan, C. L. Melcher and M. Zhuravleva, *Optical Materials*, 2022, **133**, 112912.
22. A. Ohnishi, M. Kitaura, M. Itoh and M. Sasaki, *Journal of the Physical Society of Japan*, 2012, **81**, 114704.
23. A. Ohnishi, M. Kitaura, T. Otomo and M. Sasaki, *Journal of the Physical Society of Japan*, 2003, **72**, 2400-2401.
24. K. Takahashi, M. Arai, M. Koshimizu, Y. Fujimoto, T. Yanagida and K. Asai, *Japanese Journal of Applied Physics*, 2020, **59**, 072002.
25. N. Yahaba, M. Koshimizu, Y. Sun, T. Yanagida, Y. Fujimoto, R. Haruki, F. Nishikido, S. Kishimoto and K. Asai, *Applied Physics Express*, 2014, **7**, 062602.
26. N. Hurley, F. Moretti, H. Yan, E. Bourret-Courchesne, Y. S. Chu and S. S. Wong, *J. Mater. Chem. C*, 2020, **8**, 8622-8634.
27. K. Takahashi, M. Arai, M. Koshimizu, Y. Fujimoto, T. Yanagida and K. Asai, *Japanese Journal of Applied Physics*, 2020, **59**, 032003.
28. C. S. Gibbons, V. C. Reinsborough and W. A. Whitla, *Canadian Journal of Chemistry*, 1975, **53**, 114-118.
29. T. W. Couch and G. P. Smith, *The Journal of Chemical Physics*, 1970, **53**, 1336-1347.
30. M. H. Brooker and C.-H. Huang, *Materials Research Bulletin*, 1980, **15**, 9-16.
31. M. A. Macdonald, E. N. Mel'chakov, I. H. Munro, P. A. Rodnyi and A. S. Voloshinovsky, *Journal of Luminescence*, 1995, **65**, 19-23.
32. G. Shwetha, V. Kanchana and G. Vaitheeswaran, *Journal of Solid State Chemistry*, 2015, **227**, 110-116.
33. L. M. Bollinger and G. E. Thomas, *Review of Scientific Instruments*, 1961, **32**, 1044-1050.
34. T. Szcześniak, M. Moszyński, A. Synfeld-Każuch, Ś. Ł, M. A. S. Koschan and C. L. Melcher, *IEEE Trans. Nucl. Sci.*, 2010, **57**, 1329-1334.
35. M. Grodzicka, M. Moszyński, T. Szczęśniak, A. Syntfeld-Każuch, ł. Świderski, A. F. Zerrouk and J. Owczarczyk, *Nuclear Instruments and Methods in Physics Research Section A: Accelerators, Spectrometers, Detectors and Associated Equipment*, 2011, **652**, 226-230.
36. M. Bertolaccini, S. Cova and C. Bussolatti, *in proceedings of International Symposium on Nuclear Electronics. Versailles, France*, 1968.
37. G. Kresse and J. Furthmüller, *Comp Mater Sci*, 1996, **6**, 15-50.
38. G. Kresse and J. Furthmüller, *Physical Review B*, 1996, **54**, 11169-11186.
39. J. P. Perdew, A. Ruzsinszky, G. I. Csonka, O. A. Vydrov, G. E. Scuseria, L. A. Constantin, X. Zhou and K. Burke, *Physical Review Letters*, 2008, **100**, 136406.
40. J. Heyd, G. E. Scuseria and M. Ernzerhof, *The Journal of Chemical Physics*, 2003, **118**, 8207-8215.
41. P. E. Blöchl, *Physical Review B*, 1994, **50**, 17953-17979.
42. *Journal of Applied Crystallography*, 2011, **44**, 1272--1276.
43. J. A. McGinnety, *Inorganic Chemistry*, 1974, **13**, 1057-1061.
44. R. D. Shannon, *Acta Crystallogr. Sect. A*, 1976, **32**, 751-767.
45. K. Fejfarova, R. Ouarsal, B. El Bali, M. Dusek and M. Lachkar, *Acta Crystallographica Section E*, 2007, **63**, i136-i137.
46. B. F. Markov, *Zh. Obshch. Khim*, 1955, **25**.
47. H.-J. Seifert and G. Thiel, *Zeitschrift für anorganische und allgemeine Chemie*, 1977, **436**, 237-243.
48. P. Chartrand and A. D. Pelton, *Canadian Metallurgical Quarterly*, 2001, **40**, 13-32.
49. H. Yin, J. Song, W. Liu and B. Hu, *Calphad*, 2022, **79**, 102476.
50. V. N. Makhov, *Physica Scripta*, 2014, **89**, 044010.
51. C. W. E. van Eijk, *Journal of Luminescence*, 1994, **60-61**, 936-941.

52. A. S. Voloshinovskii, V. B. Mikhailik and P. A. Rodnyi, *Radiat. Meas.*, 1995, **24**, 383-385.
53. G. A. Appleby, A. Edgar and G. V. M. Williams, *Journal of Applied Physics*, 2004, **96**, 6281-6285.
54. S. Kubota, J.-z. Ruan, M. Itoh, S. Hashimoto and S. Sakuragi, *Nuclear Instruments and Methods in Physics Research Section A: Accelerators, Spectrometers, Detectors and Associated Equipment*, 1990, **289**, 253-260.
55. M. Ahtee, *Lattice constants of some binary alkali halide solid solutions*, Suomalainen Tiedeakatemia, 1969.
56. G. L. McPherson, T. J. Kistenmacher and G. D. Stucky, *The Journal of Chemical Physics*, 2003, **52**, 815-824.
57. P. A. Rodnyi, *Radiat. Meas.*, 2001, **33**, 605-614.
58. I. Kamenskikh, M. MacDonald, V. Mikhailin, I. Munro and M. Terekhin, *Review of scientific instruments*, 1992, **63**, 1447-1449.
59. M. A. Terekhin, V. N. Makhov, A. I. Lebedev and I. A. Sluchinskaya, *Journal of Luminescence*, 2015, **166**, 137-142.
60. Y. Chornodolskyy, G. Stryganyuk, S. Syrotyuk, A. Voloshinovskii and P. Rodnyi, *Journal of Physics: Condensed Matter*, 2007, **19**, 476211.
61. M. Cadatal-Raduban, K. Yamanoi, A. Yoshikawa, Y. Yokota, T. Shimizu, N. Sarukura, T. Togashi, A. Kondo and M. V. Luong, *The Journal of Chemical Physics*, 2021, **154**.
62. M. Cadatal-Raduban, A. Yoshikawa, L. V. Mui, M. H. Pham, T. Shimizu, N. Sarukura, T. Togashi and K. Yamanoi, *Japanese Journal of Applied Physics*, 2020, **59**, 052005.
63. G. Shwetha and V. Kanchana, *Journal of Physics: Condensed Matter*, 2019, **31**, 115501.
64. A. P. Shpak, O. A. Glike, A. G. Dmitriev, P. A. Rodnyi, A. S. Voloshinovskii and S. M. Pidzyrailo, *Journal of Electron Spectroscopy and Related Phenomena*, 1994, **68**, 335-338.
65. J. Yang, S. Falletta and A. Pasquarello, *npj Computational Materials*, 2023, **9**.
66. J. Mooney and P. Kambhampati, *The Journal of Physical Chemistry Letters*, 2013, **4**, 3316-3318.